





S-CO₂ radial turbine testing data and performance map for thermodynamic conditions with strong real gas effect

Seungkyu Lee
 M.S. Student
 KAIST
 Daejeon, Korea

Jeong Ik Lee*
 Professor
 KAIST
 Daejeon, Korea

In Woo Son
 Ph.D Candidate
 KAIST
 Daejeon, Korea

Gihyeon Kim
 Ph.D Student
 KAIST
 Daejeon, Korea

	<p>Seungkyu Lee is a Ph.D student of Nuclear and Quantum Engineering department in KAIST. He has two years of experience in designing and modeling of S-CO₂ turbomachinery for various applications and operating S-CO₂ Brayton cycle test loop.</p>
	<p>Gihyeon Kim is a Ph.D student in the Nuclear Power and Propulsion Laboratory at KAIST. His research topic is control systems of S-CO₂ power cycles. He is currently working to experimentally demonstrate control logic for integrated and autonomous control of S-CO₂ power cycles.</p>
	<p>In Woo Son is a senior researcher at KAERI. He is currently working in the Nuclear Hydrogen Research Section. His research interests include High-Temperature Gas-cooled Reactor (HTGR) system design and thermal fluid experiments.</p>
	<p>Jeong Ik Lee* is a professor of Nuclear and Quantum Engineering department in KAIST. He has been leading the development of the supercritical carbon dioxide cycle in Korea.</p>

ABSTRACT

Supercritical carbon dioxide (S-CO₂) can be used as a working fluid in the Brayton cycle, offering advantages such as compactness, simplicity, and high efficiency over conventional steam Rankine and helium Brayton cycles. Until now, research has focused on S-CO₂ compressors with near-critical design inlet state. Thus, S-CO₂ turbomachine can behave differently from ideal gases, such as air and helium, when real gas effects are strong. Predicting and evaluating off-design performance maps for S-CO₂ turbomachinery requires an appropriate real gas model. In the previous studies, experimental results were analyzed for three different compressors, and the Pham model was selected as the most suitable model to predict the enthalpy rise and efficiency of S-CO₂ radial compressors by considering the compressibility factor (Z) and real gas volume exponent (n_s). To the best of our knowledge, the performance map for radial flow turbines has never been fully obtained and shared in public domain by other research institutions. In addition, an appropriate real gas model for S-CO₂ inlet radial turbines has not been presented. In this paper, the pressure ratio curve and enthalpy reduction of a S-CO₂ radial inflow turbine are presented. In addition, the five real gas models were compared with a similitude analysis in terms of pressure ratio and enthalpy reduction, and the most appropriate real gas model was selected. Two methods were used to draw the performance curve map of the radial inflow turbine. First, it was done by using the KAIST-TMD, a one-dimensional turbomachinery design code, especially suitable for S-CO₂. Second, the Autonomous Brayton Cycle (ABC) test loop and a turbine-alternator-compressor (TAC) were operated to obtain experimental data to confirm the predicted map.

INTRODUCTION

Supercritical carbon dioxide (S-CO₂) can be used as the working fluid of the Brayton cycle for various heat sources, such as nuclear fission, waste heat, and solar energy [1]. This cycle has powerful advantages such as compactness, simplicity, and higher efficiency than the conventional steam Rankine cycle and helium Brayton cycle in a wide range of turbine inlet temperatures [2]. There are several S-CO₂ power cycle experimental facilities at SNL, SWRI, S-CO₂-HeRO, KAERI, and KAIST [3]–[7].

Currently, systems that combine nuclear fission as a heat source with a supercritical carbon dioxide Brayton cycle as a power generation system are being explored in KAIST. Conventional marine vessels are mainly powered by diesel engines, which are particularly carbon dioxide-intensive compared to other engines. As a result, research is being conducted to apply nuclear power to commercial marine propulsion and offshore power generation systems. The shift in application from large nuclear power plants to small nuclear power plants and merchant marine propulsion systems means that load variation must be analyzed [8]. Systems with large load variation are characterized by frequent changes in heat and power output, which means that turbomachinery operates under conditions that vary widely and continuously from the design conditions of temperature, pressure, and mass flow [9]. Since it is not possible to perform computational fluid dynamics (CFD) for the large number of inlet conditions under which the rotor may operate, the only option is to apply a real gas model or an ideal gas model to predict the behavior of the compressor and turbine to perform a transient analysis of the load-varying system [10].

An S-CO₂ turbomachinery behaves quite differently from ideal gas, air, and helium due to the nonlinear change of thermal properties such as compressibility factor and specific heat ratio near

the critical point [11]. However, fundamental research on turbomachinery has been focused on air and ideal gas. Therefore, it is necessary to find a proper real gas model to predict, calibrate, and design the off-design performance map of the S-CO₂ compressor and turbine. There are five main similitude models, as follows: Starting from the ideal gas model (IG) [12], there is the IGZ model [13], which adds a compressibility factor (Z), followed by the Glassman model [14] and the BNI model with critical conditions [15], and the Pham model considering the compressibility factor (Z) and the real gas volume exponent (n_s) instead of the isentropic exponent (γ) [16].

The KAIST research team investigated the characteristics of compressor performance maps using three different compressors and compared five real gas models by similitude analysis [17]. The similitude analysis groups the results of various diameters and revolutions per minute (PRM) of radial turbomachines and derives pressure ratio curves and enthalpy rise curves combining flow parameters and speed parameters. As a result, the IGZ model was selected as the most suitable model considering the compressibility factor and specific heat ratio, which predict precisely the enthalpy rise and efficiency of the S-CO₂ radial type compressor [17].

Recent research has focused on plotting performance maps for compressors [18]. However, as far as the authors are aware, the experimental performance maps for radial flow turbines have not been shared in public domain by other research organizations. In this paper, the pressure ratio curve and enthalpy decrease curve of a radial flow turbine with supercritical carbon dioxide as the working fluid are presented. In addition, the five real gas models presented above are compared with the similitude analysis method in terms of pressure ratio and enthalpy decrease, and the most suitable real gas model is selected. The radial inflow turbine performance curve map was created using two techniques. One technique is using the KAIST-TMD, a one-dimensional turbomachinery design code specifically for S-CO₂. The other is obtaining experimental data from a turbine-generator-compressor (TAC) installed at the Autonomous Brayton Cycle (ABC) test loop constructed and operating in KAIST [7].

Radial Inflow Turbine

Radial inflow turbine is more suitable than axial turbine for power cycle with a small power output of 10 MW electric or less. As with compressors and axial turbines, the velocity triangle and the Euler work equation govern turbine operation and performance. As shown in figure 1, the working fluid passes through each part of the radial inflow turbine in the following order: volute, nozzle, and rotor. The velocity triangles for the nozzle and rotor inlet and exit are also displayed in Figure 1. Here, h_o denotes stagnation enthalpy, C is absolute speed, U is blade speed, and W is relative speed. Subscripts: 1 is the volute inlet, 2 is the nozzle inlet, 3 is the rotor inlet, 4 is the rotor outlet, and m is the meridional. The difference between the velocities of the blades multiplied by the tangential absolute velocity of the fluid becomes the stagnation enthalpy difference at the turbine inlet and outlet. And the stagnation enthalpy difference becomes the power, or thrust, generated by the turbine. In general, a Cw_4 value is designed to be zero for greater power output from a turbine of the same size at the same RPM [19].

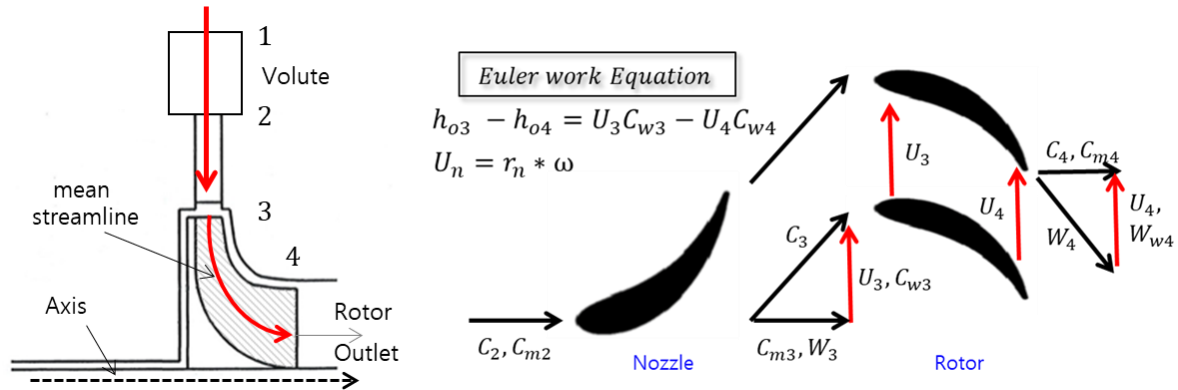


Figure 1. Euler work equation (left) and velocity triangle of turbine nozzle and rotor (right)

There are several losses in a radial turbine, as shown in Figure 2. Internal losses affect both pressure ratio and efficiency, while external losses affect only efficiency. Nozzle, incidence, and disk friction loss models have been calibrated in the previous compressor studies [18]. However, the windage loss behavior of S-CO₂ is quite different from traditional air-based models. This is because the specific heat ratio of supercritical carbon dioxide is nonlinear and has much different value than the specific heat ratio of air. Kim and Lee calibrated Mack's windage loss model to apply to the S-CO₂ turbomachinery [20].

It is noted that for a shrouded type rotor, there is a leakage flow that occurs between the shroud and stator. This loss is included in the external loss and does not affect the pressure ratio or pressure drop of the rotor performance. Also, this loss contributes to the work loss, but it is included in the windage loss. The leakage mass flow rate is designed to be 1.5% of the total mass flow rate through the turbine due to the eye seal between the shroud and stator. However, since the major surface area is dominated by the rotor shaft surface area, the friction loss associated with the leakage flow and the shroud surface is expected to be minimal compared to the total windage loss.

Unlike the other losses, rotor passage losses occur only in the rotor of the turbine, so it was not possible to calibrate this loss for S-CO₂ in the compressor study. However, rotor passage losses are large enough to account for 20% of the total turbine loss, and close to half of the internal losses alone [21].

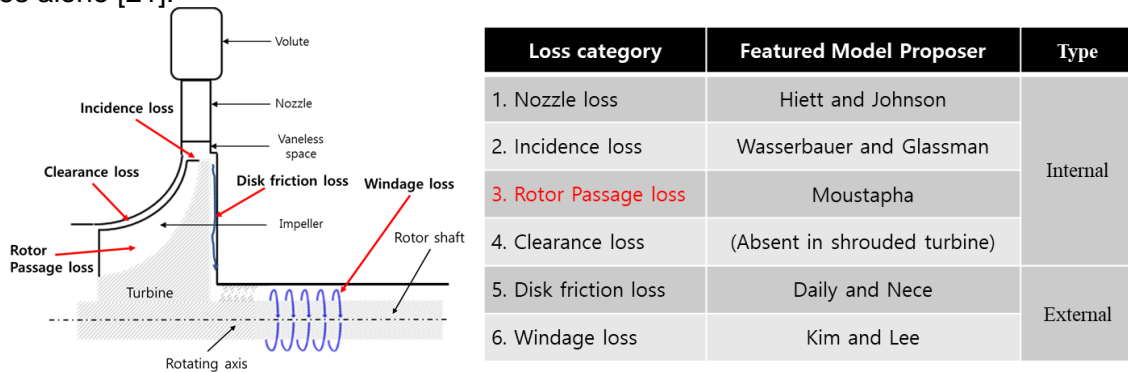


Figure 2. Losses in radial turbine (left) and its featured model proposer (right)

Analysis tool - The KAIST-TMD

The KAIST research team developed KAIST-TMD, a 1-D mean streamline code for turbomachinery design and performance prediction [22]. Generating the required geometry and estimating the machine's performance are challenging tasks in the early stages of design. The 1-D mean streamline method has been used previously. The bulk of fluid in a turbomachine flows from the inlet to the outlet, despite the path's three-dimensional complexity. As a result, velocity triangles are utilized to represent three-dimensional flow in one dimension. The equations of continuity and energy conservation are simplified by applying the concept of velocity triangles. Equation (1), which is known as the Euler turbomachinery equation, shows the kinetic energy gain due to the impeller rotation, and Equation (2) is continuity equation.

$$h_{03} - h_{04} = U_3 C_{w3} - U_4 C_{w4} \quad (1)$$

$$\dot{m} = \rho(h_s, P_s)AV \quad (2)$$

Since the fluid behavior is represented with 1-D flow in the KAIST-TMD code, the description of the working fluid above assumes a perfect fluid flow without irreversibility. There is a secondary flow effect that is irreversible and cannot be described by velocity triangles alone. The 1-D mean streamline method should adopt empirical loss models to account for irreversibility. Loss models play a major role in how well the 1-D mean streamline technique predicts the performance of a turbomachinery. Numerous organizations have created custom 1-D mean streamline codes for the design.

To measure rapidly changing thermal properties correctly, the KAIST-TMD code additionally links the NIST-Refprop property database [23]. By using this property database, even when the state is becoming closer to the critical point, two known properties can exactly complete other properties. This code first determines the radius of the rotor using Balje's n_s - d_s diagram [24]. Then, it draws the velocity triangles of the blade inlet and outlet and calculates the additional enthalpy change by reflecting the loss model set. Since the velocity triangle is formed by an initial guess of the outlet density, the above process is repeated until the outlet density converges. Until a turbomachine achieves the desired pressure and maximum efficiency, this process is repeated. Detailed algorithm is shown in Figure 3.

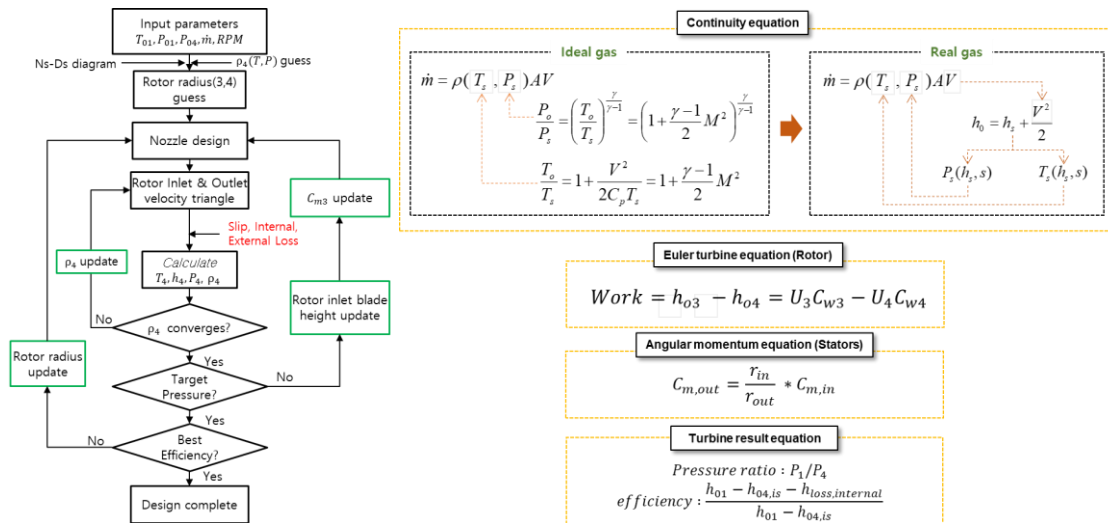


Figure 3. Code algorithm of the KAIST-TMD (left) and govern equations (right)

Gas models and similitude analysis for off-design performance of radial turbine

As mentioned before, there are many situations when a turbine operates at off-design condition, which the inlet temperature, mass flow rate, pressure is not the same with the designed inlet conditions. There are two input parameters in general such as mass flow rate and RPM and three output parameters such as pressure ratio or expansion ratio, enthalpy difference, and isentropic efficiency. These parameters can be converted into non-dimensional parameter which is shown in Equation (3) ~ (7). Moreover, this parameter converting process can be reduced with Buckingham Π theorem as shown in Equation (8). This method to relate all of these inlet parameters to outlet parameters could reduce excessive amounts of numerical simulations and experiments. In particularly high-temperature experiments requiring hundreds of degrees Celsius, this method has the significant advantage that the rotor can be operated under realistic temperature conditions to approximate the results of the desired conditions [25].

$$\frac{\dot{m}\sqrt{\gamma RT_{in}}}{\gamma P_{in}} \quad ; \text{ Flow parameter} \quad (3)$$

$$\frac{N}{\sqrt{\gamma RT_{in}}} \quad ; \text{ Speed parameter} \quad (4)$$

$$\frac{P_{out}}{P_{in}} = PR \quad ; \text{ Pressure ratio} \quad (5)$$

$$\frac{\Delta H}{\gamma RT_{in}} \quad ; \text{ Head parameter} \quad (6)$$

$$\frac{h_{in} - h_{out}}{h_{in} - h_{out, is}} = \eta \quad ; \text{ Efficiency} \quad (7)$$

$$fn\left(\frac{\dot{m}\sqrt{\gamma RT_{in}}}{\gamma P_{in}}, \frac{N}{\sqrt{\gamma RT_{in}}}\right) = PR, \frac{\Delta H}{\gamma RT_{in}}, \eta \quad (8)$$

The above presented method applied Ideal Gas model (IG). However, when properties are non-linear in wide range of temperature and pressure, IG model is not suitable to predict turbine off-design performance.

The five well-known gas models those are used to predict the off-design performance of turbomachinery are presented in Table 1 [12]–[16]. The IG model is the foundation of all other gas model equations. Compressibility factor (Z), which is included in the IGZ model, has a significant impact on the compressor's pressure ratio. By substituting critical temperature and critical pressure for temperature and pressure, the Glassman model modifies the inlet and outlet variables. The Pham model substitutes the real gas volume exponent (n_s) for the specific heat ratio in the IGZ model. The n_s is similar to the specific heat ratio, but no ideal gas assumptions were used in the process of deriving it. This property is more appropriate than the specific heat ratio when the off-design point is much far from the design point for heat exchangers, turbomachinery, and even internal combustion engines [26]. When a fluid approaches sonic velocity, it is said to be in a critical condition. The critical condition temperature and pressure can be calculated via the formula in the 4th row, and the last column of Table 1. The BNI model includes compressibility (Z) from Glassman model. The relationships between the five models are depicted in Figure 4.

Table 1. Summary of parameters for existing similitude models

	Flow parameter	Speed parameter	Head parameter	Pressure parameter	Efficiency parameter	
IG	$\frac{\dot{m}\sqrt{\gamma RT}}{\gamma P}$	$\frac{N}{\sqrt{\gamma RT}}$	$\frac{\Delta H}{\gamma RT}$	PR	η	
IGZ	$\frac{\dot{m}\sqrt{\gamma ZRT}}{\gamma P}$	$\frac{N}{\sqrt{\gamma ZRT}}$	$\frac{\Delta H}{\gamma ZRT}$			
Glassman	$\frac{\dot{m}\sqrt{\gamma RT_{cr}}}{\gamma P_{cr}}$	$\frac{N}{\sqrt{\gamma RT_{cr}}}$	$\frac{\Delta H}{\gamma RT_{cr}}$			$T_{cr} = T\left(\frac{2}{\gamma+1}\right), P_{cr} = P\left(\frac{2}{\gamma+1}\right)^{-\frac{\gamma}{\gamma+1}}$
BNI	$\frac{\dot{m}\sqrt{\gamma ZRT_{cr}}}{\gamma P_{cr}}$	$\frac{N}{\sqrt{\gamma ZRT_{cr}}}$	$\frac{\Delta H}{\gamma ZRT_{cr}}$			$T_{cr} = T\left(\frac{2}{\gamma+1}\right), P_{cr} = P\left(\frac{2}{\gamma+1}\right)^{-\frac{\gamma}{\gamma+1}}$
Pham	$\frac{\dot{m}\sqrt{n_s ZRT}}{n_s P}$	$\frac{N}{\sqrt{n_s ZRT}}$	$\frac{\Delta H}{n_s ZRT}$			$n_s = \gamma \frac{\rho}{P} \left(\frac{\partial P}{\partial \rho}\right)_T$

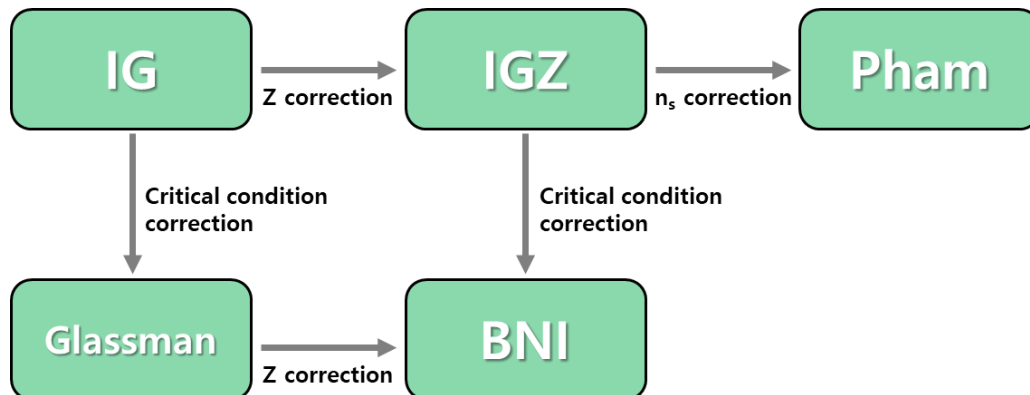
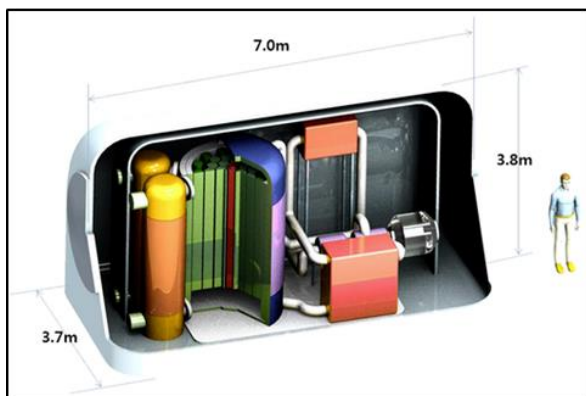


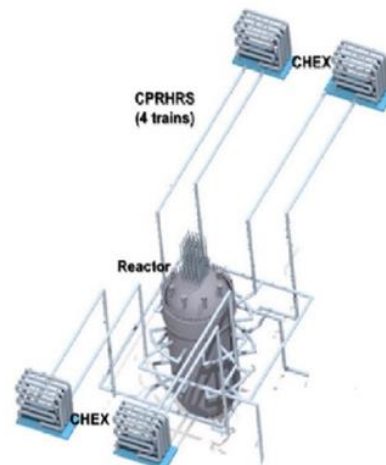
Figure 4. Flow chart of similitude model development

Methodology – Off-design performance map from KAIST-TMD code

To estimate the most accurate gas model using the KAIST-TMD code, the similarity method was used by applying the turbines designed in two S-CO₂ power systems. One S-CO₂ power system is the KAIST-MMR, and the other is a passive residual heat rejection system (PRHRS). The KAIST-MMR is a micro modular reactor designed by the KAIST research team, and the design inlet condition of the turbine in this system is 550 °C and 20 MPa [27]. The PRHRS is a residual heat removal cooling system that operates passively in the event of a reactor accident. As auxiliary system of a small nuclear power plant, this system is activated when the power generation system fails or highly loaded or when a reactor accident results in high temperature conditions inside the reactor. The high temperature and pressure of CO₂ from head of nuclear reactor drives the turbine, which drives the compressor, causing the passive circulation of the residual heat removal cooling system. The design inlet condition of the turbine in this system is 200 °C and 11.5 MPa. The illustrations of these two S-CO₂ systems are show in Figure 5 [28].



KAIST-MMR



S-CO₂ PRHRS for SMR

Figure 5. Illustration of the KAIST-MMR (left) and PRHRS for SMR (right)

The similitude analysis is used to select the most appropriate real gas model of S-CO₂ radial turbine while utilizing KAIST-TMD [22]. An example of this process using the KAIST-MMR turbine and IG model is shown in Figure 6.

1. Design a turbine with the highest efficiency that satisfies the inlet and outlet conditions of the turbine using the KAIST-TMD. The design method is described in the 'Analysis tool - the KAIST-TMD' section.
2. Plot the design and off-design performance map of the designed turbines. The input parameters are mass flow rate and RPM, and the output parameters are enthalpy difference and pressure ratio.
3. Mass flow rate is converted to dimensionless parameter such as flow parameter, RPM as speed parameter, and enthalpy difference as head parameter. Pressure ratio is not converted because it is already a dimensionless parameter.
4. Overlap the output parameters calculated at the design point and off-design point on one graph. To best overlap the curves on the graph, the inlet conditions at the off-design point were previously adjusted using the inverse of the dimensionless formula.
5. Compare the graphs and compare the errors of each RPM and flow parameter.

- Example) KAIST-MMR turbine
- Design condition : 550°C, 200bar
- Off-design condition : 500°C, 200bar
- Real gas model : IG model

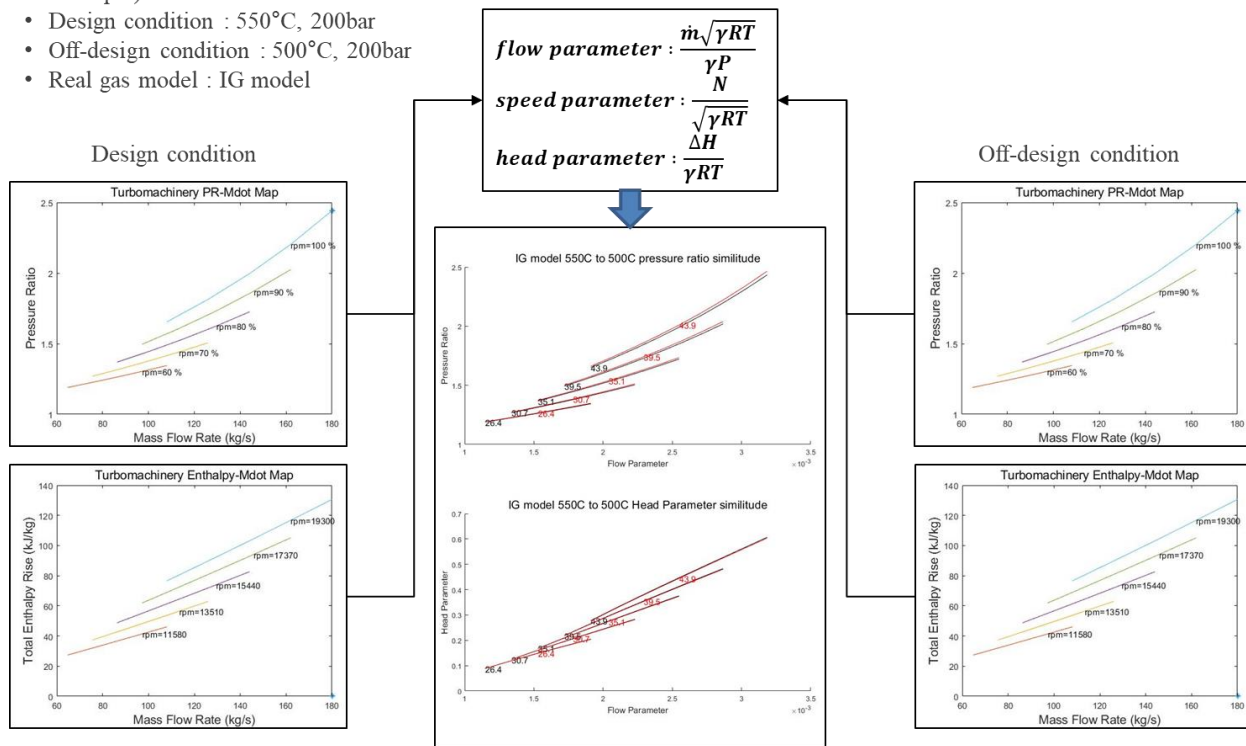


Figure 6. The ABC test loop

Result and discussion – Prediction off-design performance via the KAIST-TMD code

The prediction errors of the off-design performance of the KAIST-MMR turbine using five real gas models are summarized in Table 2. Design condition of radial inflow turbine is 550 °C, 20 MPa, and 180 kg/s. Five off-design conditions kept the pressure the same as the design condition, but reduced the temperature by 50 degrees Celsius.

In general, if the off-design conditions were further away from the design condition, the error becomes larger. For the pressure ratio prediction, the Glassman, BNI, and Pham models showed a small error than the IG and IGZ models. However, when dimensionless head parameter was predicted, the IGZ model predicted well with the Pham model. The head parameter and pressure ratio were both accurately predicted by the Pham model. This is a result of the turbine's high operating temperature, high operating pressure, and above 90% turbine isentropic efficiency. The behavior of components with high temperature and pressure, high output, and close to an isentropic process, the real gas volume exponent used by the Pham model performs better than the specific heat ratio, which does not vary rapidly at high temperature and high pressure. The Glassman model did not predict the head parameter well. The Glassman model assumes the fluid inside the turbine to be at the speed of sound, and the Mach number of a S-CO₂ turbine does not converge to 1, unlike an air turbine, due to its high density.

Table 2. Pressure ratio error (left) and Head parameter error (right) of the KAIST-MMR turbine

Pressure Ratio	IG	IGZ	Glass man	BNI	Pham	550°C, 200bar, Z:1.034	Head Parameter	IG	IGZ	Glass man	BNI	Pham	550°C, 200bar, Z:1.034
cond1	0.59	0.60	0.37	0.37	0.42	500°C, 200bar, Z:1.027	cond1	0.50	0.43	0.32	0.62	0.39	500°C, 200bar, Z:1.027
cond2	1.35	1.36	0.82	0.84	0.93	450°C, 200bar, Z:1.018	cond2	1.34	0.88	0.92	1.31	0.81	450°C, 200bar, Z:1.018
cond3	3.77	3.82	2.22	2.27	2.37	350°C, 200bar, Z:0.988	cond3	4.58	1.97	3.50	3.09	1.75	350°C, 200bar, Z:0.988
cond4	9.33	9.49	5.17	5.31	5.29	250°C, 200bar, Z:0.924	cond4	12.31	3.41	10.00	5.98	2.87	250°C, 200bar, Z:0.924
cond5	16.02	16.35	8.36	8.46	8.63	200°C, 200bar, Z:0.864	cond5	19.97	4.42	16.57	8.60	3.55	200°C, 200bar, Z:0.864
Average (%)	6.21	6.32	3.39	3.45	3.53		Average (%)	7.74	2.22	6.26	3.92	1.87	

The prediction errors of the off-design performance of the PRHRS turbine using five real gas models are summarized in Table 3. Design condition of radial inflow turbine is 200 °C and 11.5 MPa. Three off-design conditions were set, with increasingly lower temperatures and pressures compared to the design condition.

Compared to the KAIST-MMR turbine, the pressure ratio prediction error of the PRHRS turbine with the real gas model is lower overall. This is because the KAIST-MMR turbine has a design pressure ratio of 2.5, while the PRHRS turbine has a design pressure ratio of only 1.15. Lower design pressure ratio has the effect of making the prediction error to appear lower. When predicting the pressure ratio and head parameter, the IG model showed significantly high errors compared to other gas models when head parameter was predicted. This is because the operating conditions of the PRHRS turbine are much closer to the critical point than the KAIST-MMR, and in fact, the compressibility factors of the design and off-design points are between 0.66 and 0.9. Therefore, the IG model without the compressibility factor in the dimensionless parameters is bound to have a large prediction error. The Pham model, which considers both the compressibility factor and the real gas volume exponent, predicts both pressure ratio and head parameter with high accuracy for the PRHRS turbine.

Table 3. Pressure ratio error (left) and Head parameter error (right) of the PRHRS turbine

Pressure Ratio	IG	IGZ	Glass man	BNI	Pham	200°C, 115bar, Z:0.906	Head Parameter	IG	IGZ	Glass man	BNI	Pham	200°C, 115bar, Z:0.906
cond1	0.63	0.65	0.32	0.34	0.06	130°C, 100bar, Z:0.825	cond1	9.13	0.10	7.69	1.67	0.00	130°C, 100bar, Z:0.825
cond2	1.51	1.55	0.73	0.77	0.11	90°C, 90bar, Z:0.748	cond2	18.03	0.23	15.04	3.76	0.01	90°C, 90bar, Z:0.748
cond3	3.07	3.16	1.34	1.41	0.16	60°C, 80bar, Z:0.663	cond3	27.88	0.46	22.90	6.99	0.01	60°C, 80bar, Z:0.663
Average (%)	1.74	1.78	0.80	0.84	0.11		Average (%)	18.35	0.27	15.21	4.14	0.01	

Experimental facility - The ABC test loop and S-CO₂ TAC

The performance evaluation of the compressor and turbine with magnetic bearing TAC was conducted utilizing the Autonomous Brayton Cycle (ABC) test loop built at KAIST. The ABC test loop is an experimental device for supercritical carbon dioxide cycles with the layout of a closed loop simple recuperated Brayton S-CO₂. This research facility was built to perform integrated tests on simple recuperated S-CO₂ cycles. The equipment mainly consists of a magnetic bearing supported turbo alternator compressor (TAC), pneumatic automatic control valves at the compressor inlet and outlet, electric turbine bypass valves, a printed circuit heat exchanger

(PCHE) type recuperator, electric cartridge type heaters, and two types of precoolers: a PCHE type precooler and a shell and tube type precooler. The two types of precoolers can be configured in series, parallel, or stand-alone by adjusting manual valves. Figure 7 shows the front view and schematic diagram of ABC test loop.

The ABC test loop, as the name suggests, aims to automate the testing and control of a cycle by utilizing the computerized data input and output. The ABC test loop included the following features. Pressure, temperature, and mass flow rate of each flow path are converted to digital signals and transmit them to the computer in real time. Perform testing and control of the device based on operator input and data received with the computer. Figure 8 shows the control panel of the ABC test loop built with LabView. In addition, physical quantities that cannot be directly measured in real time, such as the enthalpy and entropy of a fluid or the efficiency of a heat exchanger, are calculated in real time by integrating the NIST REFPROP property database into LabView [23]. For control and optimization, where complex calculations are required, calculations can be performed using Python code based on measurement data. Finally, for the analysis of the energy required by the TAC, a power analyzer is integrated into the system to measure data on the electricity input to run the TAC in real time.

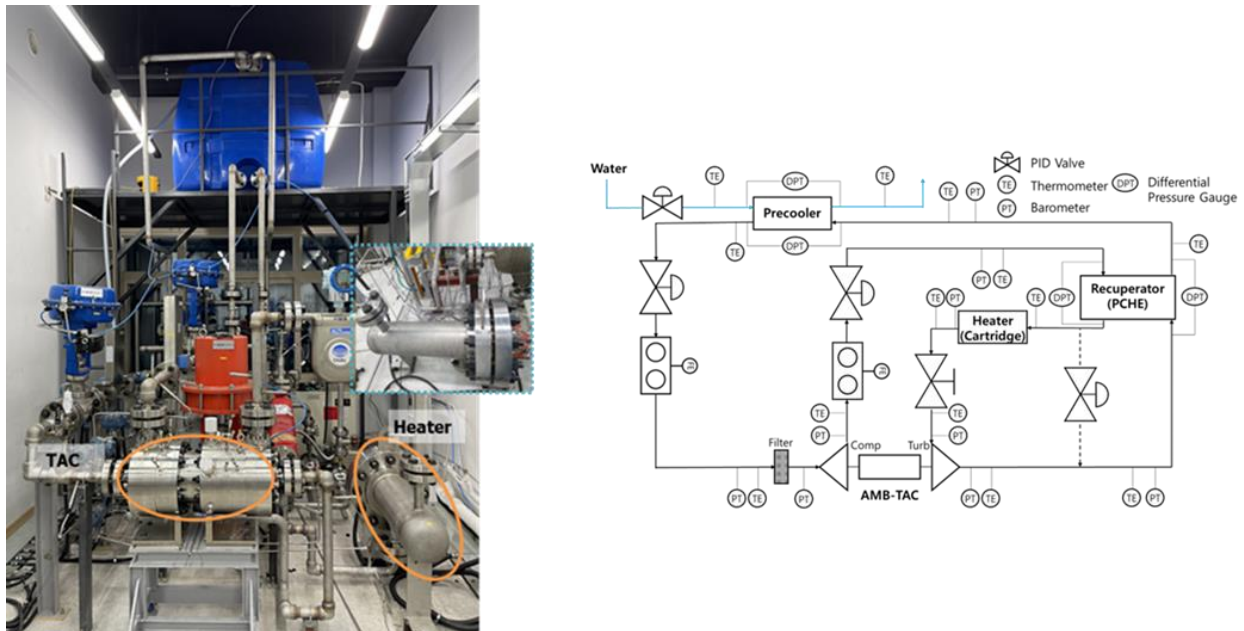


Figure 7. Front view of ABC test loop (Left), Schematic diagram of ABC test loop (Right)

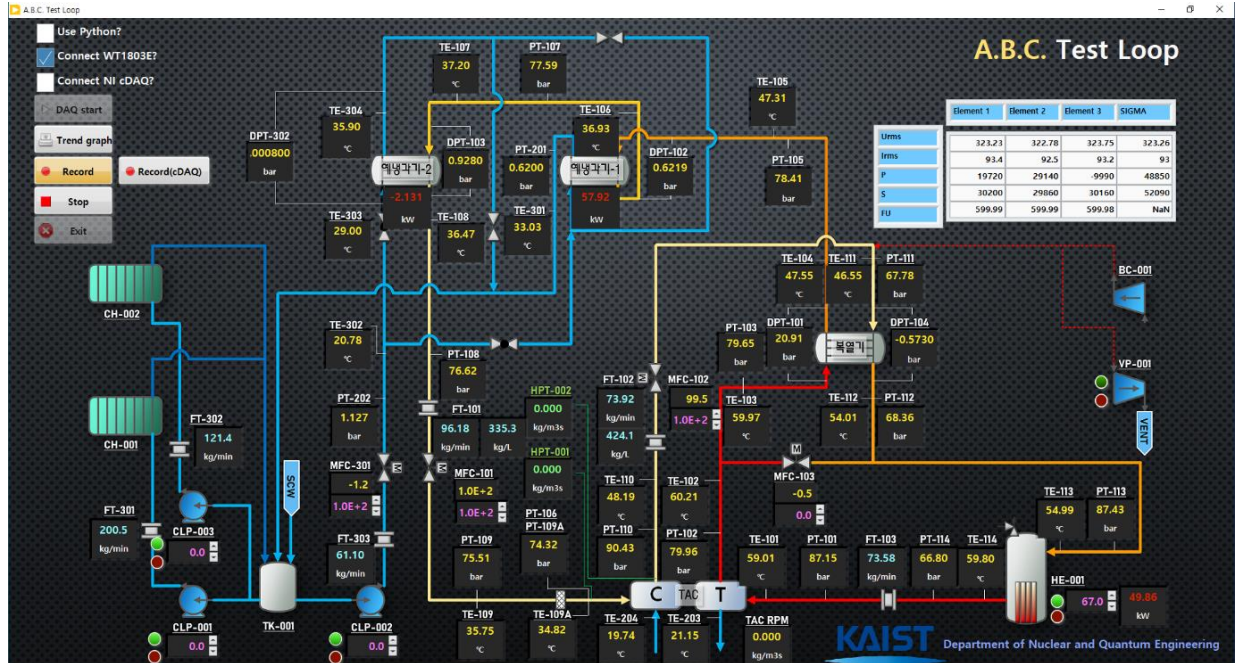


Figure 8. Control Panel of ABC test loop

RESULTS AND DISCUSSION – Experimental section

A time series graph of the results of the experiment with TAC up to the design speed of 36,000 RPM is shown in Figure 9. The experiment lasted approximately 2 hours, with the first 40 minutes spent matching the total CO₂ mass in the closed loop and converging the inlet conditions of the compressor and turbine. Data from converging time is excluded from Figure 9. As can be seen in Figure 9, the results of mass flow rate, turbine pressure ratio and leakage-flow rate are obtained from 12,000 RPM and to the rotational speed up to 36,000 RPM which is the design RPM of S-CO₂ TAC. The x-axis is the recorded time, y-axis on the left shows the mass flow rate (kg/min) and leakage-flow rate (%), y-axis on the right shows the pressure ratio of the turbine. The leakage-flow ratio is the ratio of the mass flow rate inside the TAC to the total flow and is shown in Equation 9. TAC supported by magnetic bearings is inevitably designed with a gap between the rotor and stator housing, resulting in a leakage-flow phenomenon where some of the flow from the back end of the compressor flows into the front of the turbine.

$$\frac{m_{i01} - m_{i02}}{m_{i01}} \quad ; \text{Leakage-flow ratio} \quad (9)$$

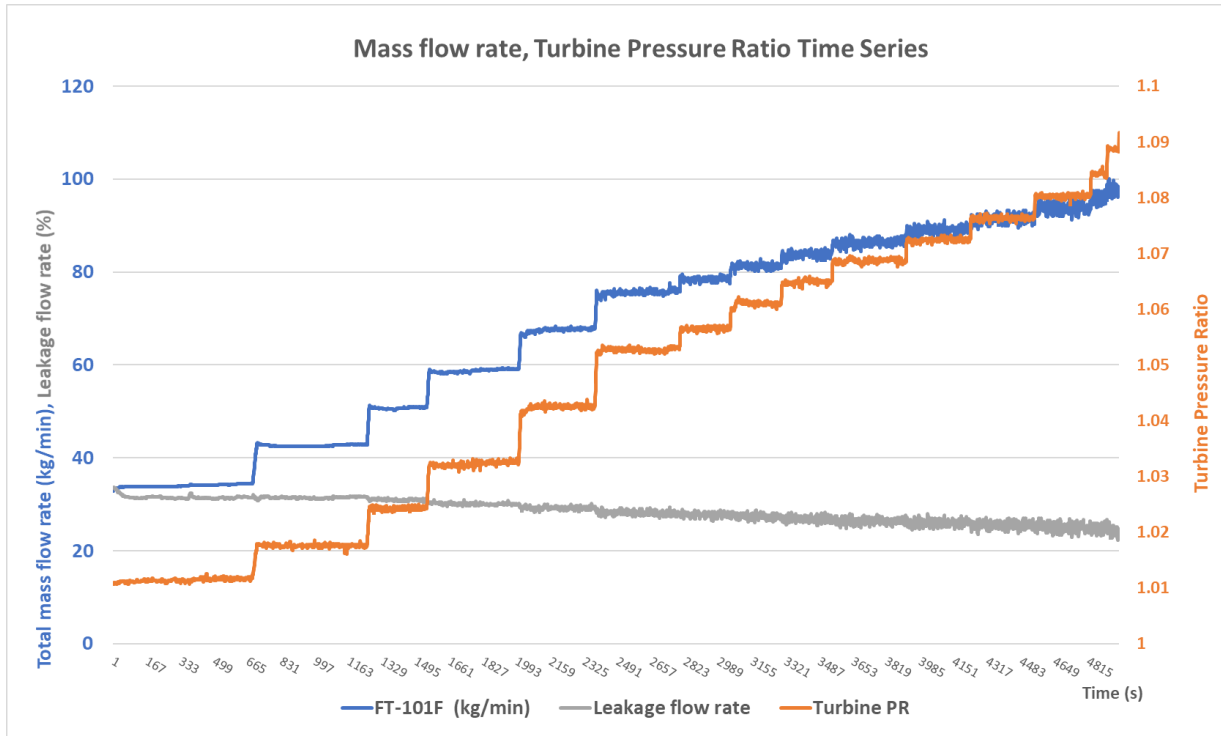


Figure 9. Time series of mass flow rate, leakage flow rate and turbine PR

The speed was initially raised with increments of 3,000 RPM until reaching 27,000 RPM. After 27,000 RPM, RPM was continuously increased with 1,000 RPM step. From 27,000 RPM to 36,000 RPM, the mass flow is shown to be fluctuating. The most common cause of mass flow fluctuations in the closed loop at a fixed RPM is due to the change in the compressor inlet conditions. However, as shown in Figure 10 and Table 4, the inlet pressure and temperature conditions of the compressor and turbine were stable over the entire range, especially at higher RPMs. It can be concluded that the mass flow rate fluctuation is not caused by the turbomachinery's inlet fluctuation. Another factor of fluctuating mass flow in the closed loop is the compressor. The S-CO₂ TAC adopts active magnetic bearings to support the rotating shaft. The S-CO₂ TAC is equipped with three magnetic bearings: two radial bearings located on either side of the compressor and turbine, and one axial bearing located near the turbine. Also, at high RPMs, the control and position of the magnetic bearings were often unstable. Of the three bearings, the radial bearing that supports the turbine side has the greatest fluctuation. When the bearings' vibrations were analyzed using the FFT technique, the turbine side radial bearing had the peak frequency of vibration for 70 micrometers at 36,000 RPM. The peak vibration of the other bearings was in the range of 30 micrometers. Therefore, the compressor and turbine capacities changed due to the rotating shaft fluctuation. As a result, the overall mass flow rate of the cycle, as well as the leakage flow rate and the leakage flow rate ratio, changed.

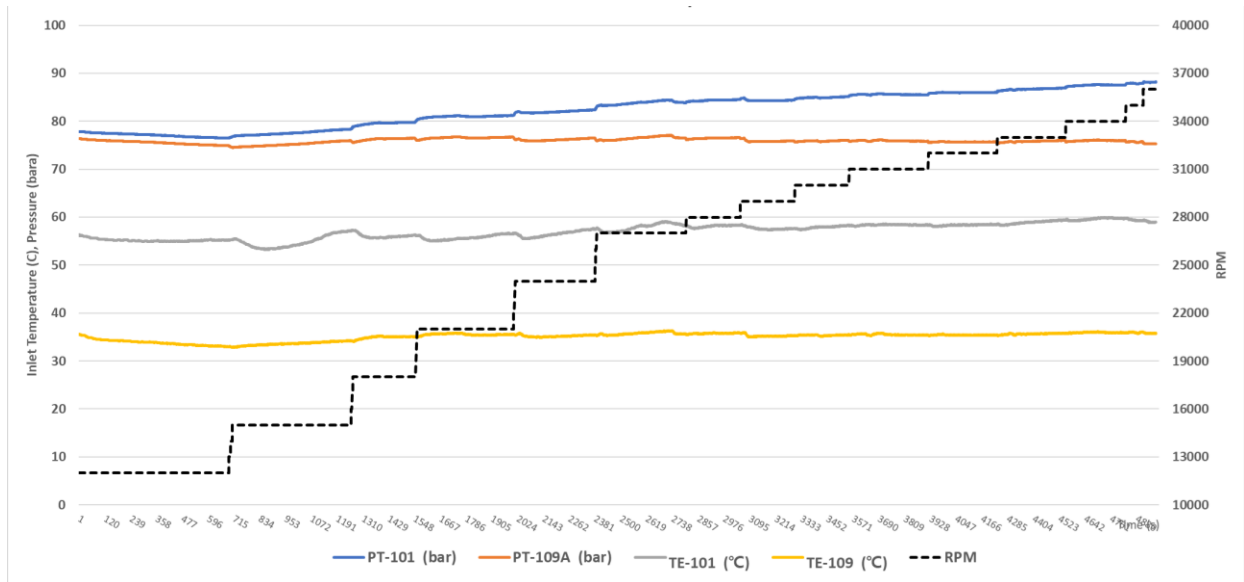


Figure 10. Steady inlet conditions for compressor and turbine

Table 4. Standard deviation of inlet conditions and mass flow rate for each RPM

RPM	Comp Inlet Temp stdev (°C)	Comp Inlet Pressure stdev (bar)	Turbine Inlet Temp stdev (°C)	Turbine Inlet Pressure stdev (bar)	Mass flow rate stdev (kg/min)
12,000	1.64	0.49	0.29	3.65	0.26
15,000	1.25	0.42	1.25	0.44	0.19
18,000	0.39	0.23	0.39	0.24	0.21
21,000	0.49	0.15	0.49	0.17	0.33
24,000	0.63	0.19	0.63	0.20	0.44
27,000	0.75	0.34	0.75	0.37	0.46
28,000	0.23	0.10	0.23	0.12	0.40
29,000	0.28	0.17	0.28	0.15	0.50
30,000	0.26	0.09	0.26	0.11	0.57
31,000	0.11	0.09	0.11	0.08	0.64
32,000	0.13	0.04	0.13	0.05	0.67
33,000	0.34	0.14	0.34	0.17	0.79
34,000	0.22	0.09	0.22	0.11	0.90
35,000	0.16	0.07	0.16	0.05	1.02
36,000	0.18	0.05	0.18	0.04	0.97

Overall data is summarized in Table 5. The mass flow rate is linearly proportional to the RPM. This is a common behavior in the closed-loop rotating machinery operation, so it confirms that the instrumentation, such as the flow meter, is measuring accurately. It also means that the design of the compressor with supercritical carbon dioxide as the working fluid was correct. Additionally, the pressure increase and pressure decrease of the compressor were found to be proportional to the square of the RPM. This is also a normal behavior of rotating machinery.

Table 5. Full range RPM test average data summary

RPM	Turbine PR	Comp PR	Leakage flow rate (%)	Mass flow rate (kg/min)	Comp Pressure increase (bar)	Turb Pressure decrease (bar)	Motor Power (kW)
12,000	1.011	1.024	31.52	33.97	1.84	0.87	2.82
15,000	1.018	1.038	31.44	42.64	2.86	1.34	5.20
18,000	1.024	1.053	30.95	50.75	4.06	1.89	8.46
21,000	1.032	1.071	30.09	58.75	5.47	2.53	12.60
24,000	1.042	1.095	29.23	67.51	7.23	3.34	17.91
27,000	1.053	1.119	28.17	75.61	9.14	4.20	24.23
28,000	1.057	1.129	27.77	78.46	9.85	4.51	26.56
29,000	1.061	1.140	27.37	81.27	10.60	4.85	28.99
30,000	1.065	1.149	26.87	83.75	11.33	5.18	31.56
31,000	1.069	1.159	26.44	86.38	12.10	5.50	34.24
32,000	1.072	1.170	26.02	89.04	12.88	5.80	36.99
33,000	1.076	1.181	25.55	91.39	13.68	6.15	39.93
34,000	1.080	1.191	25.08	93.78	14.52	6.51	42.99
35,000	1.084	1.202	24.81	95.93	15.32	6.83	46.03
36,000	1.089	1.214	24.34	97.82	16.12	7.18	49.01

The mass flow rate of the turbine was regulated using the MFC-101 shown in Figure 8, an automatic pneumatic valve located at the front of the compressor. The experiment was conducted at 24,000 RPM, 27,000 RPM, 30,000 RPM, and 33,000 RPM to plot the pressure ratio map, pressure drop map, and work map of the turbine. The experiment was performed twice at each RPM, and reproducible results were obtained for all RPM and mass flow rate ranges. First, the pressure ratio-mass flow graphs obtained at four different RPMs are shown in Figure 11. It can be observed from Table 6 that the test was conducted where the turbine inlet temperature is near 60 degrees of Celsius and turbine inlet pressure ranging from 77 to 88 bars, which indicates that the real gas effect will be still prominent since the test conditions are close to the critical point.

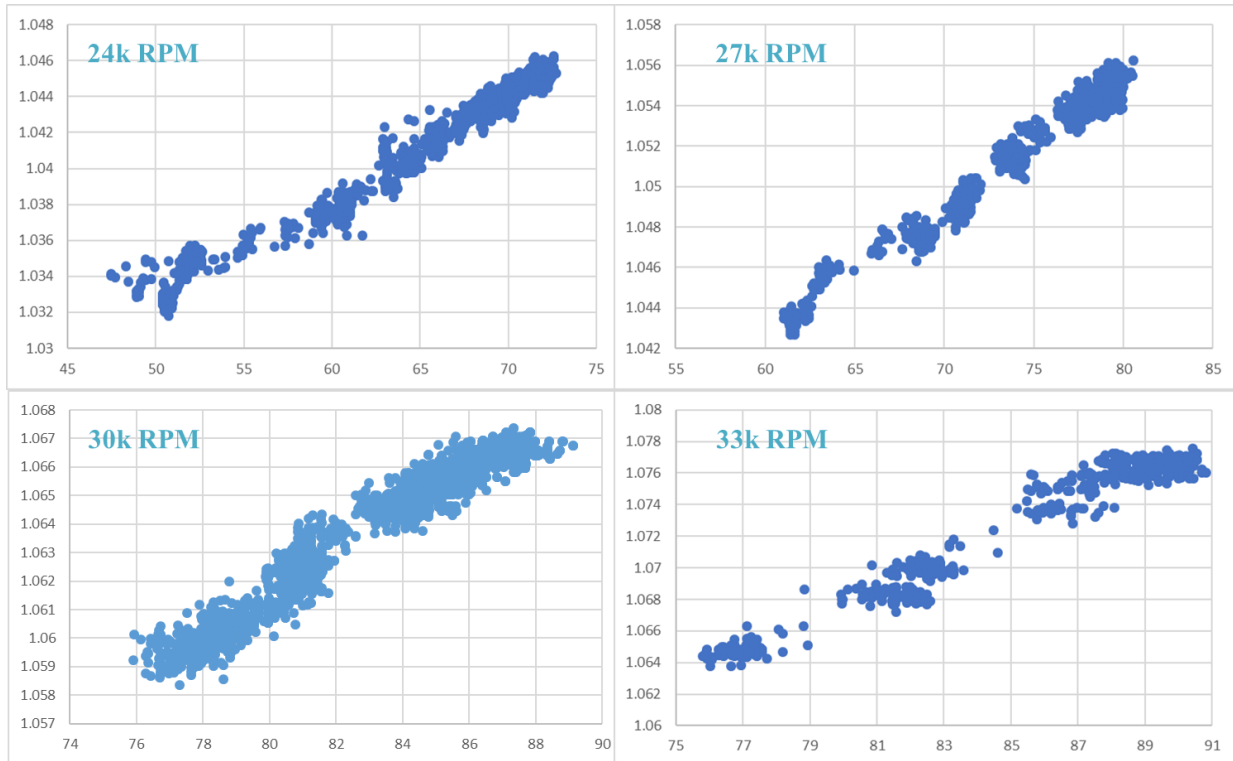


Figure 11. Pressure ratio-mass flow rate curve of radial turbine at each RPM

However, it is also shown in Table 6 that for high RPM cases the turbine inlet temperature becomes lower than the turbine outlet temperature (highlighted in a red box). This seems to be non-physical value, but the reason is because of the secondary flow coming from compressor outlet to turbine inlet which experiences a large windage loss (i.e. friction heating). Thus, the turbine inlet temperature is not correctly measuring the actual turbine inlet temperature since the measurement is performed before the secondary flow merges with the main flow, thus the enthalpy from the secondary flow is not reflected in the measured turbine inlet temperature. The main flow and the secondary flow configuration of the tested TAC is shown in Figure 12 for better understanding. Although would be better to measure pressure and temperature of secondary flow, it isn't possible to measure these properties in small clearance secondary flow path. Therefore, the enthalpy from the secondary flow had to be corrected and this was performed with the newly developed windage loss model suggested in Ref. [29] as shown in Equations 10 to 12. Since the outlet density in Eq. 10 is unknown, the density and enthalpy of the secondary flow were converged by following an algorithm shown in Figure 13. The enthalpy of secondary flow ($h_{leakage}$) before merging with the main flow can be obtained from Equation 13 where $Q_{cooling}$ is mainly the heat loss from TAC via cooling water jacket to maintain temperature for magnetic core. In addition, conduction, convection, and radiation heat transfer at the surface of TAC is also a part of $Q_{cooling}$. From the $h_{leakage}$, h_{101} , and turbine inlet pressure, the corrected turbine inlet temperature can be calculated utilizing NIST-REFPROP property database. The corrected turbine inlet temperature is shown in Table 7.

This approach was used to obtain the performance map of the radial turbine from the data generated from the ABC test loop. However, it is recognized that this seems to be still an indirect way of measuring the efficiency of the radial turbine since the major enthalpy is not correctly

measured in the loop. Therefore, in the future a method to correctly measure the turbine inlet condition will be further implemented to the ABC test loop to remove this issue.

$$W_{windage} = \pi * C_{f,corr} * \frac{\rho_{inlet} + \rho_{outlet}}{2} * r_{shaft}^4 * \left(\frac{RPM * 2\pi}{60}\right)^3 * L_{shaft} \quad (10)$$

$$C_{f,corr} = \frac{1.8}{Ta_{crit}^{0.4} * C_r^{-1.25}} * \frac{(1 + c_r)^2}{(1 + c_r)^2 - 1} * Ta_{inlet}^{-0.1} * \left(\frac{\gamma_{inlet}}{\gamma_{air}}\right)^{-0.4051} \quad (11)$$

$$Ta_{crit}^{0.4} = \left(\frac{RPM * 2\pi}{60}\right)^2 * r_{rotor} * \frac{c^3}{v_{inlet}^2} \quad (12)$$

$$W_{windage} - Q_{cooling} = (\dot{m}_{101} - \dot{m}_{102})(h_{leakage} - h_{110}) \quad (13)$$

Table 6. Turbine testing conditions

RPM	Turbine Inlet Temp (°C)	Turbine Outlet Temp (°C)	Turbine Inlet Pressure (bar)	Turbine Outlet Pressure (bar)
12,000	55.22	46.91	77.11	76.25
15,000	54.85	47.28	77.59	76.25
18,000	56.05	49.75	79.57	77.68
21,000	55.76	51.34	81.00	78.47
24,000	56.53	52.95	82.00	78.66
27,000	57.93	55.50	83.84	79.65
28,000	58.13	56.24	84.37	79.85
29,000	57.68	56.18	84.38	79.53
30,000	57.90	56.81	84.95	79.78
31,000	58.39	57.73	85.59	80.09
32,000	58.36	58.13	85.98	80.17
33,000	58.92	59.10	86.71	80.56
34,000	59.63	60.24	87.52	81.01
35,000	59.44	60.39	87.90	81.07
36,000	59.07	60.32	88.16	80.97

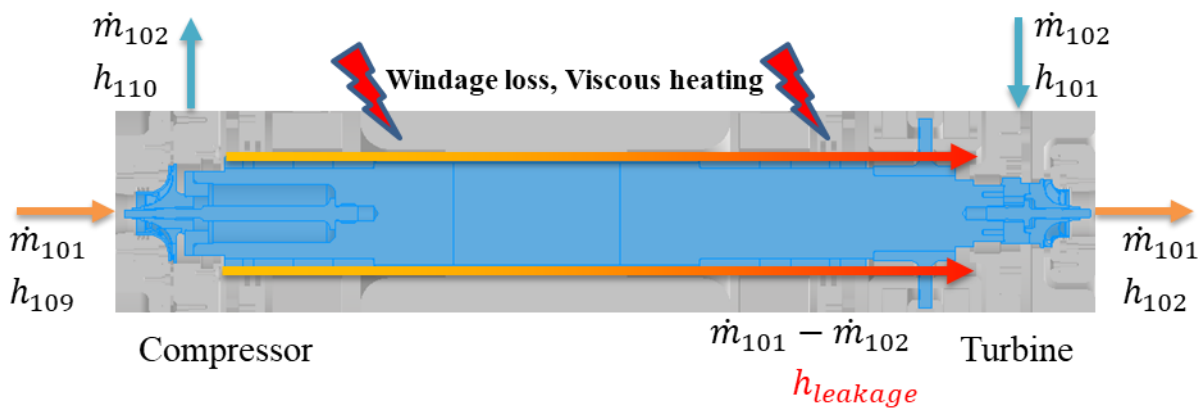


Figure 12. Flow configuration around TAC in ABC test loop

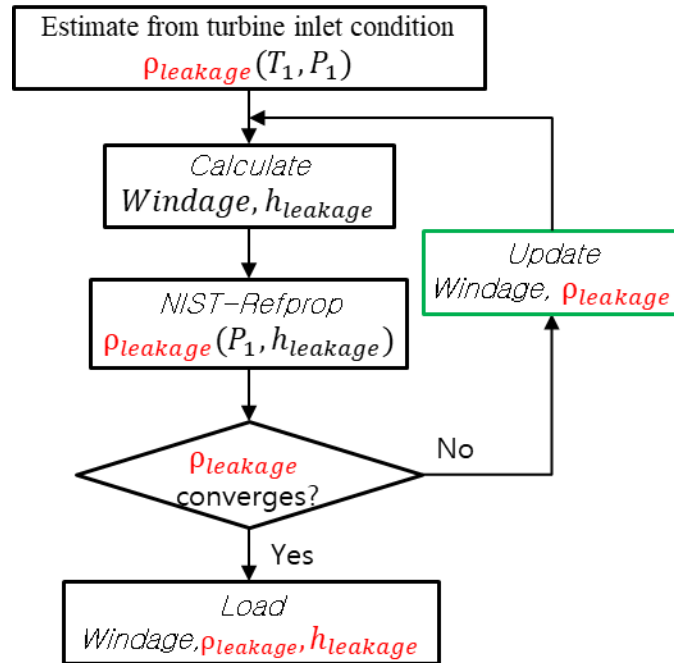


Figure 13. Iteration method obtaining enthalpy and density of secondary flow

Table 7. Turbine testing conditions with corrected turbine inlet temperature

RPM	Turbine Inlet Temp (°C)	Corrected Turbine inlet Temp (°C)	Turbine Outlet Temp (°C)	Turbine Inlet Pressure (bar)	Turbine Outlet Pressure (bar)
12,000	55.22	47.71	46.91	77.11	76.25
15,000	54.85	48.77	47.28	77.59	76.25
18,000	56.05	51.51	49.75	79.57	77.68
21,000	55.76	53.91	51.34	81.00	78.47
24,000	56.53	56.50	52.95	82.00	78.66
27,000	57.93	60.17	55.50	83.84	79.65
28,000	58.13	60.57	56.24	84.37	79.85
29,000	57.68	60.68	56.18	84.38	79.53
30,000	57.90	62.11	56.81	84.95	79.78
31,000	58.39	63.19	57.73	85.59	80.09
32,000	58.36	64.19	58.13	85.98	80.17
33,000	58.92	65.86	59.10	86.71	80.56
34,000	59.63	67.40	60.24	87.52	81.01
35,000	59.44	68.02	60.39	87.90	81.07
36,000	59.07	68.52	60.32	88.16	80.97

To determine the actual gas effects of the experimental conditions, the NIST-REFPROP property database was used. The compressibility factor of the corrected temperature and pressure given in Table 6 is in the range of 0.6~0.666, which indicates that the real gas effect is

strong. It is noted that the compressibility factor of the PRHRS turbine inlet is about 0.7~0.9 as shown in Figure 14, and the compressibility factor of a typical S-CO₂ Brayton cycle compressor inlet condition is 0.35~0.5.

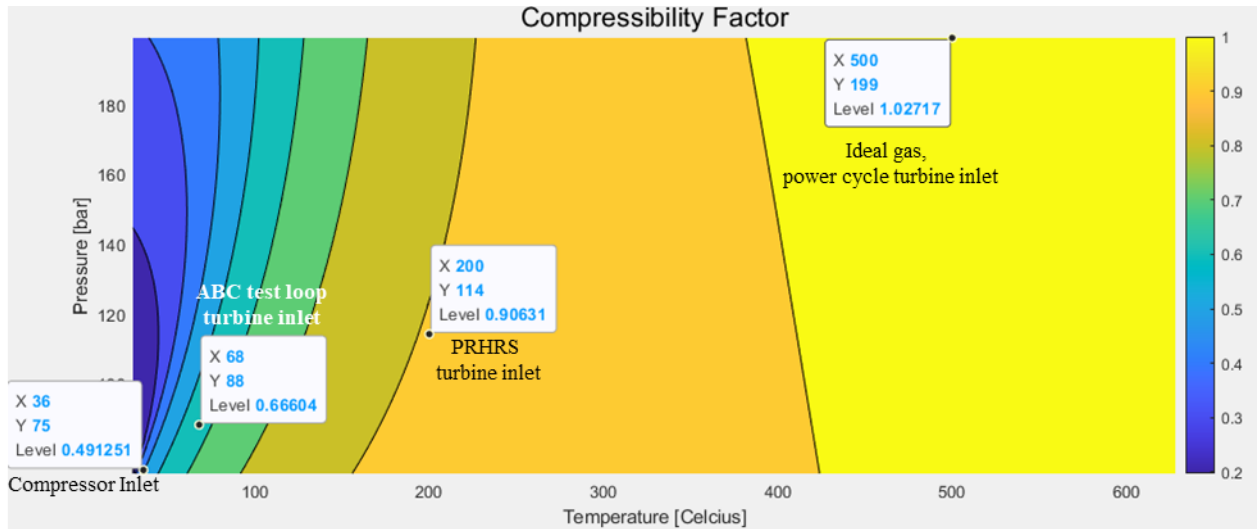


Figure 14. Compressibility factors of various S-CO₂ turbomachinery

Using the similitude analysis described earlier, the measured mass flow rate can be converted to the corrected mass flow rate. Among the five models, the mass flow rate was converted using the Pham model, and the pressure ratio map, pressure drop map, and work map are shown in Figures 15, 16, and 17, respectively. Since the enthalpy of supercritical carbon dioxide changes significantly with a small temperature difference, it can be seen that the uncertainties in the work of the turbine is larger than the uncertainties in the pressure ratio or pressure difference.

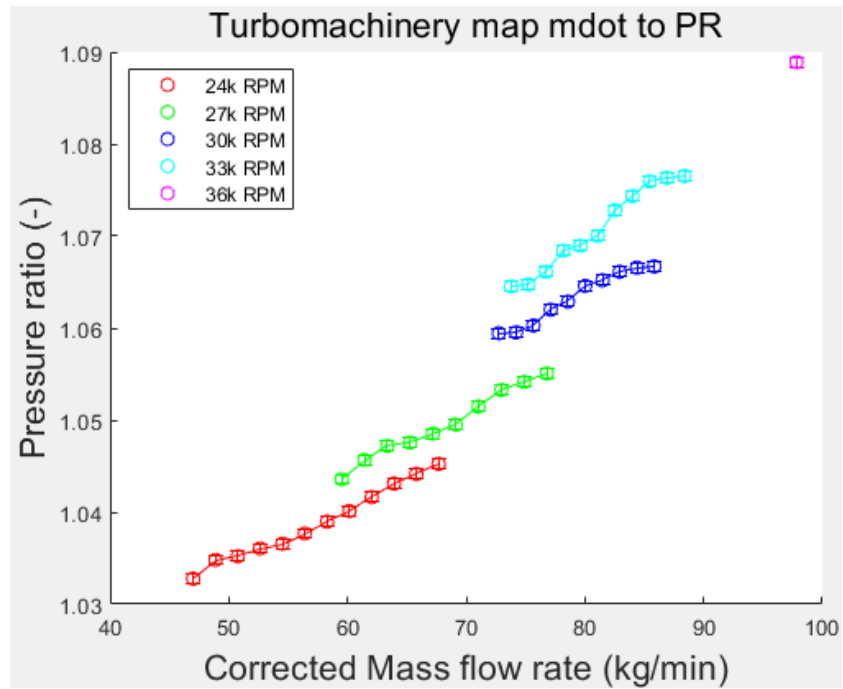


Figure 15. Pressure ratio-corrected mass flow rate map of a radial turbine

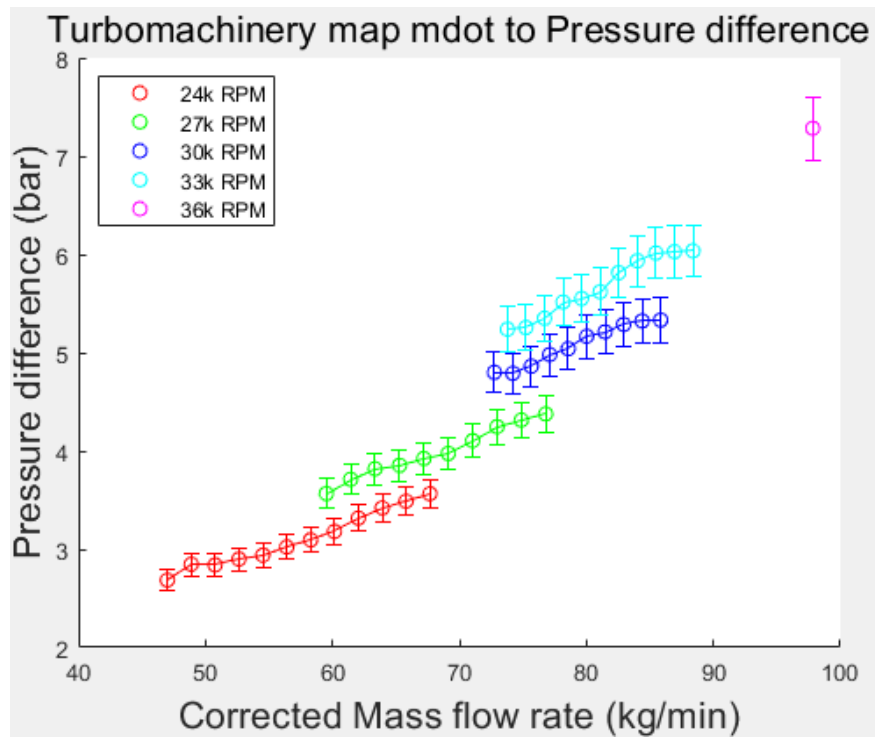


Figure 16. Pressure difference-corrected mass flow rate map of a radial turbine

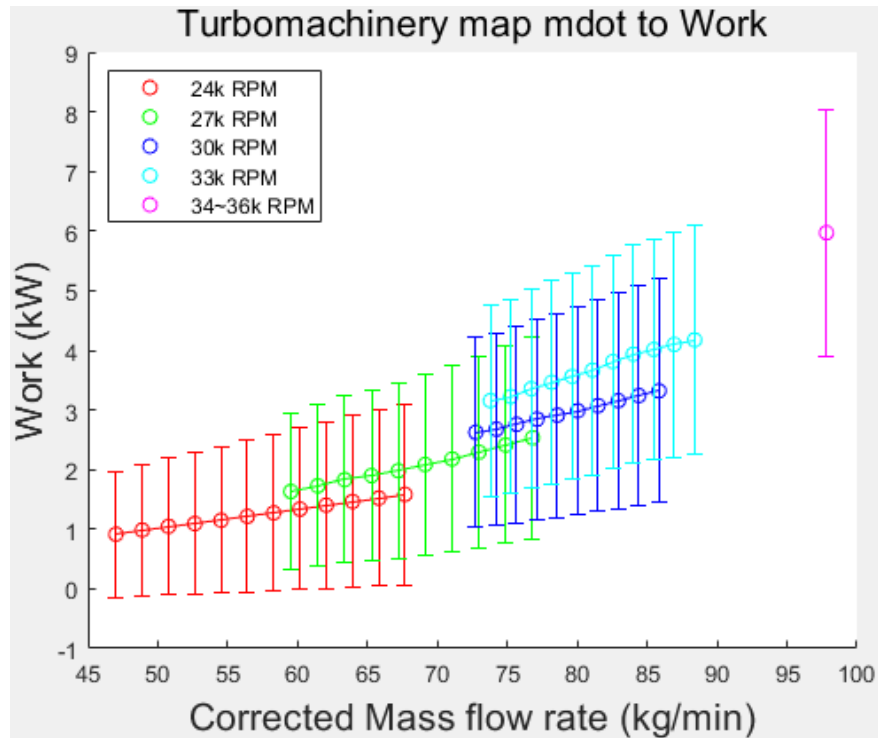


Figure 17. Work-corrected mass flow rate map of a radial turbine

SUMMARY AND FUTURE WORKS

The off-design performance prediction of the turbomachinery due to load variation is essential to perform a transient cycle analysis. This paper introduces the governing equations, velocity triangle, and losses of the radial inflow turbine. Five real gas models and the similitude analysis methods were also introduced. The KAIST-TMD code for designing S-CO₂ turbomachinery was described, and the code was utilized to predict the off-design performance of the S-CO₂ radial turbines used from a micro nuclear reactors and small nuclear reactors. The Pham model was selected as the best real gas model for predicting the off-design performance of the turbine utilizing the KAIST-TMD code with similitude analysis. The real gas volume exponent and the compressibility factor were the key parameters of S-CO₂ radial turbine off-design performance prediction.

A radial turbine was tested in the ABC test loop in KAIST. The experimental data without valve adjustment was checked to verify the physical condition. The shaft vibration caused a 2-3% fluctuation in mass flow rate, but generally, the pressure ratio of turbomachinery and the total mass flow rate of the ABC test loop were reasonable and did not differ significantly from the designed values of the experimental loop. The ABC test loop radial turbine reached 36,000 RPM and was able to obtain data to plot a full range radial turbine performance map. The testing was conducted at low temperature conditions where the real gas effect was strong. This condition is unconventional for S-CO₂ power cycle conditions, but it can be relevant when the S-CO₂ power cycle is used for decay heat removal in a small nuclear reactor or a micro-reactor.

However, the test data revealed that the secondary flow which experienced significant friction heating (i.e. windage) from the rotor can substantially influence the measurement where the measured turbine inlet temperature can be actually lower than the outlet temperature in some cases. This issue can be addressed by utilizing the newly developed windage loss model. This issue seemed to be important when the tested turbomachinery is small and leakage flow ratio is high (20% in this case). Furthermore, it is noted that the turbine power is in the order of a few kW but the windage loss can become 4-7 times larger than the turbine power, thus the enthalpy influx from secondary flow can be substantial for the small testing facility. The facility is expected to be upgraded in the near future to address this issue and further increase the turbine inlet temperature so that wider range of inlet conditions can be tested to examine the similitude models more thoroughly.

REFERENCES

- [1] V. Dostal, M. J. Driscoll, and P. Hejzlar, "A Supercritical Carbon Dioxide Cycle for Next Generation Nuclear Reactors," *Tech. Rep. MIT-ANP-TR-100*, pp. 1–317, 2004.
- [2] M. Persichilli, A. Kacludis, E. Zdankiewicz, and T. Held, "Supercritical CO₂ power cycle developments and commercialization: why sCO₂ can displace steam ste," *Power-Gen India Cent. Asia*, vol. 2012, pp. 19–21, 2012.
- [3] Maiti and Bidinger, "Development of a High Efficiency Hot Gas Turbo-expander and Low Cost Heat Exchangers for Optimized CSP Supercritical CO₂ Operation," *J. Chem. Inf. Model.*, vol. 552, no. 4, 2014.
- [4] A. Hacks, S. Schuster, H. J. Dohmen, F. K. Benra, and D. Brillert, "Turbomachine Design for Supercritical Carbon Dioxide Within the sCO₂-HeRo.eu Project," *J. Eng. Gas Turbines Power*, vol. 140, no. 12, 2018, doi: 10.1115/1.4040861.
- [5] J. E. Cha, S. W. Bae, J. Lee, S. K. Cho, J. I. Lee, and J. H. Park, "Operation Results of a Closed Supercritical CO₂ Simple Brayton Cycle," *5th Int. Supercrit. CO₂ Power Cycles Symp.*, pp. 1–10, 2016, [Online]. Available: <https://sci-hub.st/http://sco2symposium.com/papers2016/Testing/085paper.pdf>
- [6] S. a Wright, R. F. Radel, M. E. Vernon, G. E. Rochau, and P. S. Pickard, "Operation and Analysis of a Supercritical CO₂ Brayton Cycle," *SANDIA Rep. SAND2010-0171*, no. September, p. 101, 2010, [Online]. Available: <http://prod.sandia.gov/techlib/access-control.cgi/2010/100171.pdf>
- [7] Y. Jeong, G. Kim, I. W. Son, S. Lee, and J. I. Lee, "Supercritical CO₂ compressor operation near stall and surge conditions," *Case Stud. Therm. Eng.*, vol. 50, p. 103499, 2023.
- [8] E. Dedes, S. R. Turnock, D. A. Hudson, and S. Hirdaris, "Possible power train concepts for nuclear powered merchant ships," 2011.
- [9] D. Alfani et al., "Part-Load Operation of Coal Fired sCO₂ Power Plants," *Proc. 3rd Eur. Supercrit. CO₂ Conf.*, pp. 1–9, 2019, doi: 10.17185/duerpublico/48897.

- [10] Y. Jeong, S. Son, S. K. Cho, S. Baik, and J. I. Lee, "Evaluation of supercritical CO₂ compressor off-design performance prediction methods," *Energy*, vol. 213, p. 119071, 2020, doi: 10.1016/j.energy.2020.119071.
- [11] K. Brun, P. Friedman, and R. Dennis, *Fundamentals and applications of supercritical carbon dioxide (sCO₂) based power cycles*. Woodhead publishing, 2017.
- [12] H. I. H. Saravanamuttoo, G. F. C. Rogers, and H. Cohen, *Gas turbine theory*. Pearson education, 2001.
- [13] N. A. Cumpsty, "Compressor aerodynamics," *Longman Sci. Tech.*, 1989.
- [14] A. J. Glassman, *Turbine design and application*, vol. 290. Scientific and Technical Information Office, National Aeronautics and Space ..., 1973.
- [15] S. A. Wright, T. M. Conboy, R. F. Radel, and G. E. Rochau, "Modeling and experimental results for condensing supercritical CO₂ power cycles.," *Sandia National Laboratories (SNL), Albuquerque, NM, and Livermore, CA ...*, 2011.
- [16] H. S. Pham et al., "An approach for establishing the performance maps of the sc-CO₂ compressor: Development and qualification by means of CFD simulations," *Int. J. Heat Fluid Flow*, vol. 61, pp. 379–394, 2016, doi: 10.1016/j.ijheatfluidflow.2016.05.017.
- [17] Y. Jeong, S. K. Cho, I. W. Son, and J. I. Lee, "Evaluation of off-design scaling methods of supercritical CO₂ compressor with experimental data," *Energy*, vol. 278, p. 127730, 2023.
- [18] S. K. Cho et al., "Optimum loss models for performance prediction of supercritical CO₂ centrifugal compressor," *Appl. Therm. Eng.*, vol. 184, no. May 2020, p. 116255, 2021, doi: 10.1016/j.applthermaleng.2020.116255.
- [19] H. Moustapha, "Axial and radial turbines," (No Title), 2003.
- [20] D. Kim, Y. Jeong, I. W. Son, and J. I. Lee, "A New Windage Loss Model for S-CO₂ Turbomachinery Design," *Appl. Sci.*, vol. 13, no. 13, p. 7463, 2023.
- [21] R. S. Benson, "A review of methods for assessing loss coefficients in radial gas turbines," *Int. J. Mech. Sci.*, vol. 12, no. 10, pp. 905–932, 1970.
- [22] S. K. Cho, S. J. Bae, Y. Jeong, J. Lee, and J. I. Lee, "Direction for high-performance supercritical CO₂ centrifugal compressor design for dry cooled supercritical CO₂ Brayton cycle," *Appl. Sci.*, vol. 9, no. 19, p. 4057, 2019.
- [23] E. W. Lemmon, I. H. Bell, M. L. Huber, and M. O. McLinden, "NIST standard reference database 23: reference fluid thermodynamic and transport properties-REFPROP, Version 10.0, National Institute of Standards and Technology," *Stand. Ref. Data Program*, Gaithersbg., 2018.
- [24] O. E. Balje, "A study on design criteria and matching of turbomachines: Part a—similarity relations and design criteria of turbines," 1962.
- [25] S. L. Dixon and C. Hall, *Fluid mechanics and thermodynamics of turbomachinery*.

Butterworth-Heinemann, 2013.

- [26] *D. A. Kouremenos and K. A. Antonopoulos, "Isentropic exponents of real gases and application for the air at temperatures from 150 K to 450 K," Acta Mech., vol. 65, no. 1–4, pp. 81–99, 1987.*
- [27] *S. K. Cho, J. Lee, S. G. Kim, and J. I. Lee, "Turbomachinery Performance Map Application for Analyzing Cycle Off-Design Behavior of KAIST MMR," 2015.*
- [28] *B. S. Oh, Y. Kim, S. J. Kim, and J. I. Lee, "SMART with Trans-Critical CO₂ power conversion system for maritime propulsion in Northern Sea Route, part 1: System design," Ann. Nucl. Energy, vol. 149, p. 107792, 2020.*
- [29] *D. Kim, Y. Jeong, I. W. Son, and J. I. Lee, "A New Windage Loss Model for S-CO₂ Turbomachinery Design," Appl. Sci., vol. 13, no. 13, p. 7463, 2023.*

ACKNOWLEDGEMENTS

This research was supported by the Challengeable Future Defense Technology Research and Development Program (No.912767601) of Agency for Defense Development in 2024.